THE JOURNAL OF PHYSICAL CHEMISTRY B

Article

pubs.acs.org/JPCB

Ab Initio Simulations and Electronic Structure of Lithium-Doped Ionic Liquids: Structure, Transport, and Electrochemical Stability

Justin B. Haskins,[†] Charles W. Bauschlicher, Jr.,[‡] and John W. Lawson*,[§]

[†]AMA Inc., Thermal Protection Materials Branch, Mail Stop 234-1, [‡]Entry Systems and Technology Division, Mail Stop 230-3, and [§]Thermal Protection Materials Branch, Mail Stop 234-1, NASA Ames Research Center, Moffett Field, California 94035, United States

ABSTRACT: Density functional theory (DFT), density functional theory molecular dynamics (DFT-MD), and classical molecular dynamics using polarizable force fields (PFF-MD) are employed to evaluate the influence of Li^+ on the structure, transport, and electrochemical stability of three potential ionic liquid electrolytes: *N*-methyl-*N*-butylpyrrolidinium bis(trifluoromethanesulfonyl)-imide ([pyr14][TFSI]), *N*-methyl-*N*-propylpyrrolidinium bis(fluorosulfonyl)imide ([pyr13][FSI]), and 1-ethyl-3-methylimidazolium boron tetrafluoride ([EMIM][BF_4]). We characterize the Li^+ solvation shell through DFT computations of $[Li(Anion)_n]^{(n-1)-}$ clusters, DFT-MD simulations of isolated Li^+ in small ionic liquid systems, and PFF-MD simulations with high Li-doping levels in large ionic liquid systems. At low levels of Li-salt doping, highly stable solvation shells having two to three anions are seen in both [pyr14][TFSI] and [pyr13][FSI], whereas solvation shells with four anions dominate in [EMIM][BF_4]. At higher levels of doping, we find the formation of complex Li-network structures that increase the frequency of four anion-coordinated solvation shells. A comparison of computational and experimental Raman spectra for a wide range of $[Li(Anion)_n]^{(n-1)-}$ clusters shows that our proposed structures are consistent with experiment. We then compute the ion diffusion coefficients and find measures from small-cell DFT-MD simulations to be the correct order of magnitude, but influenced by small system size and short simulation length. Correcting for these errors with complementary PFF-MD simulations, we find DFT-MD measures to be in close agreement with experiment. Finally, we compute electrochemical windows from DFT computations on isolated ions, interacting cation/anion pairs, and liquid-phase systems with Li-doping. For the molecular-level computations, we generally find the difference between ionization energy and electron affinity from isolated ions and interacting cation/anion pairs to provide upper and lower bounds, respectively, to experiment. In the liquid phase, we find the difference between the lowest unoccupied and highest occupied electronic levels in pure and hybrid functionals to provide lower and upper bounds, respectively, to experiment. Li-doping in the liquid-phase systems results in electrochemical windows little changed from the neat systems.

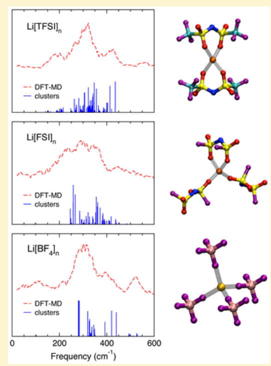

■ INTRODUCTION

Room-temperature ionic liquids have been proposed recently as electrolytes for both conventional Li-ion batteries[1−3] and advanced high-energy-density rechargeable batteries.[4−6] In conventional Li-ion batteries, ionic liquids with organic additives have been shown to be safe and stable electrolytes with comparable performance to inherently more volatile pure organic electrolytes.[1−3] Specific ionic liquid variants, particularly those containing imide-based anions, have been shown to form passivating, Li^+-permeable surface layers on high-energy-density electrode material, namely, Li-metal.[4−6] Enabling the use of Li-metal would improve the viability of advanced battery chemistries, such as lithium−sulfur and lithium−oxygen.[7,8] Thus, it is important to understand the influence of Li^+ on the structure and properties of these potential electrolytes. In that direction, an abundance of recent experimental and theoretical works have focused on the Li^+ solvation structure,[9−13] transport properties,[14−19] and electrochemical performance.[20−25]

In ionic liquids, the Li^+ solvation shell and conductivity are intimately related, with larger solvation shells generally having both a longer residence time and decreased Li^+ ionic conductivity.[18,26] When the solvating anions are relatively complex, the resulting solvation structure may not be intuitive, such as with the [TFSI] and [FSI] anions (both of which are leading candidate anions for battery electrolytes[4,6]). Along these lines, a number of joint experimental−computational studies have been performed to elucidate the solvation shell in ionic liquids having the [TFSI][9−11,13] and [FSI][12] anions. Interestingly, spectroscopic measurements indicate that Raman-active modes related to the S−N and S−O stretching modes of these anions are perturbed to higher frequency in the presence of Li^+. Using DFT to compute the Raman activity of $[Li(Anion)_n]^{(n-1)-}$ clusters, one may identify which solvation structures correlate best with the perturbed experimental frequencies and thereby estimate the coordination number, n. For [TFSI], DFT Raman activities have been determined for $n = 2$ and $n = 4$ clusters, with the $n = 2$ clusters[9−11] providing the best agreement with experimental Raman spectra. For [FSI], however, higher coordinations seem to be preferred,[12] with the computed Raman activities of $n = 3$ clusters closely agreeing

Received: July 17, 2015
Revised: September 30, 2015
Published: October 27, 2015

with experiment. Complementary high-energy X-ray diffraction studies[27] on these ionic liquids suggest tetrahedrally coordinated Li^+ ions and further lend credence to Li^+ being doubly and triply coordinated by [TFSI] and [FSI], respectively.

The diffusion coefficient of Li^+ is important when the suitability of a given electrolyte is assessed, with higher values of Li^+ diffusion implying larger Li^+ conductivity. Experimentally, diffusion coefficients of Li^+ in ionic liquids are often obtained through pulsed-field-gradient spin−echo NMR.[2,15] However, experimentally providing a full measure of transport across a wide range of temperature and Li-salt mole fraction (x_{Li}) has only been attempted for a few ionic liquids, notably those having the [TFSI] and [BF_4] anions.[16,28] Though such measurements are invaluable, MD simulations performed with polarizable force fields (PFF-MD) are an attractive alternative, having matured to the level where transport properties of neat ionic liquids[14,29−31] as well as those in the presence of Li-salts[17,26,31−33] can be determined within 20−30% of experiment. Accurately capturing the structure and energetics of the Li^+ solvation shell in a classical force field, however, can be challenging. An alternative means of obtaining transport coefficients that bypasses the need to parametrize classical force fields is through the application of density functional theory molecular dynamics (DFT-MD) simulations. Although the expense of DFT-MD limits both system size and time scale, such simulations have recently been attempted for organic electrolytes, namely, ethylene carbonate and dimethyl carbonate,[34,35] and the results from such approaches are in reasonable agreement with experiment. For ionic liquids with Li-salt doping, however, the applicability of DFT-MD to transport is an open question, as the mobility of ionic liquids is generally lower than that of organics at room temperature. This problem is further exacerbated at higher values of x_{Li}, where hundreds of picoseconds to hundreds of nanoseconds of simulation time can be required to obtain reasonable transport estimates.[26]

In addition to the aforementioned molecular-level solvation structure and transport properties, the electrochemical window sets the limits of voltage bias reasonably accessible to a battery and is therefore important for assessing the performance of an electrolyte. The electrochemical window is generally experimentally estimated by characterizing current density as a function of voltage.[36−38] Discontinuities in the current at high and low potential bias suggest electrolyte decomposition and set the anodic and cathodic limits, respectively, of the window. From a simulation standpoint, it is highly attractive to have a fundamental description of this quantity, particularly one that can be quickly determined as a screening tool,[39,40] and a number of theoretical approaches have recently been suggested to this end.[20−25,40] The most accurate, and complex, in this respect, determines the electrochemical window from the free energy change between the electrolyte and potential decomposition products. To do this, a thermodynamic cycle is employed to connect the electrolyte free energy of decomposition in the gas phase to the fully solvated reactants in the liquid phase.[24] This procedure provides good agreement with experimental electrochemical windows of various ionic liquids, which include those having imidazolium and pyrrolidinium cations and imide and tetrafluoroborate anions.[24] Alternatively, reasonable experimental agreement has also been obtained by estimating stability from the electron affinity and ionization energy of individual molecules. This has been performed on molecules both in isolation and with solvent effects[20−22] and does not require the determination of complex decomposition products. A final means of estimating electrochemical stability is from the difference between the lowest unoccupied and highest occupied unperturbed electronic states, which has shown reasonable agreement with experiment and is computationally inexpensive.[21,25]

The present work is an attempt to apply in a broad and cooperative manner zero-temperature DFT, DFT-MD, and classical PFF-MD simulations to evaluate properties that characterize electrolyte performance. These include the previously discussed Li^+ solvation shell structure, the diffusion coefficient of Li^+, and the electrochemical stability of the electrolyte as a function of x_{Li}. To benchmark these methods, we have here, as with our previous work characterizing energetic and transport properties,[26,41] considered three of the leading ionic liquid electrolyte candidates for conventional and advanced batteries: [pyr14][TFSI], [pyr13][FSI], and [EMIM][BF_4]. The high-accuracy Li^+/electrolyte structures and properties examined herein benchmark the reliability of our previous classical PFF-MD simulations[26] on these liquids. Beyond this, the *ab initio* methods employed herein yield a wealth of additional information, such as electrochemical stability, not accessible to classical force fields.

We begin our study with an investigation of the Li^+ solvation shell. DFT is employed to analyze the structure and energetics of various $[Li(Anion)_n]^{(n-1)-}$ clusters. The stability of the most promising solvation shells derived from cluster computations are then explicitly tested using 20 ps DFT-MD simulations of a single Li^+ in ionic liquid systems having 8, 10, 12, and 16 ion pairs. In conjunction with the DFT-MD studies, room-temperature PFF-MD simulations of ionic liquids having $0.05 \leq x_{Li} \leq 0.33$ are performed to quantify Li-networking effects on the solvation shells and validate experimentally derived anion coordination numbers, n. We then determine the Raman activities of the observed liquid-phase solvation shells from zero-temperature DFT cluster computations and compare our results to experiment. We then turn to an investigation of transport by extending select DFT-MD simulations to 100 ps to determine the ion diffusion coefficients, with particular focus on Li^+. Furthermore, we benchmark size and simulation length effects inherent to the DFT-MD estimates of ion diffusion through the use of PFF-MD simulations of small ionic liquid systems. Finally, we cooperatively employ zero-temperature DFT and PFF-MD to evaluate the electrochemical windows of both neat ionic liquid electrolytes and those having Li-salt. In this respect, DFT is employed to evaluate both the energetic difference between the lowest unoccupied and highest occupied molecular orbitals and the difference between ionization energy and electron affinity of isolated ions and interacting cation/anion pairs. In the liquid phase, PFF-MD is used to generate room-temperature structures of neat and Li-doped ionic liquids having 24 ion pairs, the electronic structure of which were determined to be free of size effects, that are then combined with DFT computations to provide averaged values of the energetic difference between the conduction band minimum and valence band maximum. We perform these computations with a mixture of pure and hybrid functionals.

METHODS

Clusters: DFT Computation. As a fundamental means of understanding the Li^+ solvation structure in the ionic liquids of interest here, we perform various DFT computations of isolated $[Li(Anion)_n]^{(n-1)-}$ clusters, where $2 \leq n \leq 4$. For each individual n-state, we have performed a detailed study of cluster energetics with respect to configuration, systematically probing structures with different combinations of single-fold, monodentate bonds (η^1) and 2-fold, bidentate (η^2) ligands. For each cluster, the harmonic vibrational frequencies are computed and confirmed to be real to ensure that the clusters represent stable minima. Additionally, for each harmonic frequency we compute the associated IR intensity and Raman activity. Because many of the clusters are too large to treat with high-level quantum chemical methods and large basis sets, we have performed these calculations with the B3LYP functional[42,43] in combination with the 6-31+G** basis set of Pople and co-workers.[44] In a previous work, we showed that this combination of theory and basis set provides reasonable agreement with second order Møller–Plesset perturbation theory in the complete basis set limit both for Li^+/anion interactions and for n = 2 clusters.[41] We have performed these computations with *Gaussian*09.[45]

Additionally, we have investigated the electrochemical stability of our ionic liquid electrolytes through a DFT analysis of isolated ions and interacting cation/anion pairs. The focus of our computations were 2-fold: understanding the influence of different functionals on estimated stability and a comparative assessment of multiple measures of electrochemical stability. With regard to the former, we have employed a wide variety of both pure exchange/correlation functionals, which include the exchange functional of Becke[46] with the correlation functional of Perdew and Wang (BPW91), the exchange and correlation functionals of Perdew and Wang (here termed PW91, but denoted PW91PW91 in Gaussian), the exchange and correlation functional of Perdew, Burke, and Ernzerhof (here termed simply PBE, but denoted PBEPBE in *Gaussian*),[47,48] and various hybrid functionals including the screened Coulomb functional of Heyd, Scuseria, and Ernzerhof (HSE06),[49,50] B3LYP, and M06 from Truhlar and co-workers.[51] With regard to the last, we have compared both the difference in the lowest unoccupied molecular orbital (LUMO) and highest occupied molecular orbital (HOMO) energies (ΔE_{HL}) as well as the difference between ionization energy (IE) and electron affinity (EA), given by ΔE_{IE}, to experimentally evaluated electrochemical windows as an assessment of their relationship to electrochemical stability. As with the $[Li(Anion)_n]^{(n-1)-}$ clusters, we have chosen to perform these computations with *Gaussian*09.[45]

Liquid Simulations: *Ab Initio* Molecular Dynamics. To extend the cluster computations to include the effects of temperature and explicit solvation, we have performed a set of 100 ps DFT-MD simulations on 7[pyr14][TFSI] + Li[TFSI], 9[pyr13][FSI] + Li[FSI], and 11[EMIM][BF_4] + Li[BF_4] systems at T = 363 K, at which temperature the ion mobility is such that multiple Li^+ solvation variations can be sampled within the stated 100 ps time frame. These simulations are performed with the Vienna *Ab Initio* Simulation Package (VASP)[52−55] using the frozen core all electron projector augmented wave (PAW) method[56,57] and the generalized gradient approximation of Perdew, Burke, and Ernzerhof. All DFT-MD simulations are Gamma-point computations with an energy cutoff of 400 eV, an electronic energy convergence criteria of 1×10^{-4} eV, and a time step of 0.5 fs.

Along a similar vein to the previously described electrochemical stability study on clusters, we have additionally carried out computations to determine the difference between the conduction band minimum (CBM) and the valence band maximum (VBM), given as ΔE_{VC}, of liquid-phase ionic liquids using DFT and a plane-wave basis set. In this case, we initially perform classical molecular dynamics simulations, which will be described in detail later, at T = 298 K on systems with up to 24 ionic liquid pairs to obtain trajectory information over a 6 ns simulation length. Using the trajectory information so obtained, we then choose 10 representative configurations throughout the simulation and, by performing single point DFT computations on each configuration, estimate a temperature average of ΔE_{VC}, which is akin to the value of ΔE_{HL} for single pairs. Using the largest 24 ionic liquid pair system, we then replace some cations with Li^+ to produce systems with Li-doping levels up to x_{Li} = 0.33. The same coupled classical molecular dynamics-density function theory approach for estimating ΔE_{VC} in neat ionic liquids is again performed with each of these systems to produce a temperature and explicit solvent estimate of the electrochemical window. As with ΔE_{HL}, ΔE_{VC} from liquid-phase computation is computed by employing both the pure functionals PBE and PW91 and the hybrid functionals HSE06 and B3LYP. We note that fully 3-D periodic computations with hybrid functionals having many thousands of electrons are computationally expensive and represent the upper size limit tenable with these methods an our computational resources.

Liquid Simulations: Polarizable Molecular Dynamics. Complementary to the first principles MD simulations, we have performed a suite of liquid-phase molecular dynamics simulations using the atomistic polarizable potential for liquids, electrolytes, and polymers (APPLE&P), which has been shown to offer unparalleled accuracy in both the structure–energy relationship and the transport of ionic liquids in the presence of Li-salts.[14,17,26,30,31,33,41,58,59] The polarizable force field MD (PFF-MD) simulations are performed with a modified version of the large-scale atomic/molecular massively parallel simulator (LAMMPS),[60] with the specific details of the polarizable force field implementation and MD simulations for these liquids being found in a previous work.[26] Although there are multiple purposes for the use of classical molecular dynamics in the simulation of ionic liquids, our primary purpose here is to use PFF-MD as a platform for understanding potential system size influences on the DFT-MD results. As such, throughout the present work we provide multiple comparisons of polarizable molecule dynamics simulations (PFF-MD) with measures of structure and transport derived from DFT-MD.

We have also used PFF-MD simulations as a guide to the construction of our DFT-MD cells. For a DFT-MD simulation with a given number of ion pairs, we first generate a cell of identical size with PFF-MD, employing the *NPT* ensemble to find optimal cell sizes. As such, we have determined that simulation cells with 8, 10, and 12 pairs of [pyr14][TFSI], [pyr13][FSI], and [EMIM][BF_4], respectively, provide densities in close agreement with those of large systems having 144–216 ion pairs and experiment. In agreement with our optimal sizes from PFF-MD, short 10 ps DFT-MD simulations of the ionic liquids with these sizes show close agreement with experimental densities. As density is important for the determination of transport, we use these cell sizes for our 100 ps DFT-MD simulations of diffusion. Alternatively, a variety of cell sizes (8–16 pairs) are employed with DFT-MD to understand the structural stability of the solvation shell, though we do not find any systematic differences in solvation structure between the cell sizes.

DOI: 10.1021/acs.jpcb.5b06951
J. Phys. Chem. B 2015, 119, 14705−14719

Table 1. Energetic Decomposition of $[Li^+(Anion)_n]^{(n-1)-}$ Clusters As Determined from B3LYP/6-31+G Calculations**[a]

		$[Li(TFSI)_n]^{(n-1)-}$			$[Li(FSI)_n]^{(n-1)-}$			$[Li(BF_4)_n]^{(n-1)-}$		
n	η-state	E_B	E_R	E_A	E_B	E_R	E_A	E_B	E_R	E_A
2	$2\eta^2$	184.6	60.1	−244.7	183.9	61.0	−244.9	194.2	75.7	−269.9
3	$3\eta^2$	146.5	164.5	−311.0	146.2	168.3	−314.4	147.8	210.3	−358.1
	$2\eta^2\eta^1$	149.2	152.4	−301.6	148.1	155.7	−303.7	151.3	198.8	−350.1
	$\eta^2 2\eta^1$	150.8	141.5	−292.3	148.9	144.7	−293.7	[b]		
	$3\eta^1$	146.1	133.9	−280.0	144.7	135.7	−280.3	[b]		
4	$4\eta^1$	81.6	252.2	−333.8	79.4	256.3	−335.7	59.5	340.7	−400.2

[a]Binding energy of the cluster (E_B), repulsive energy of the anions (E_R), and attractive energy between the Li^+ and the anions (E_A) are given in kcal/mol. As a rule, the lowest-energy clusters were produced when [TFSI] assumes the *trans* conformer and when [FSI] assumes the *cis* conformer in an η^2 bond and *trans* in an η^1 bond. [b]Configuration not stable.

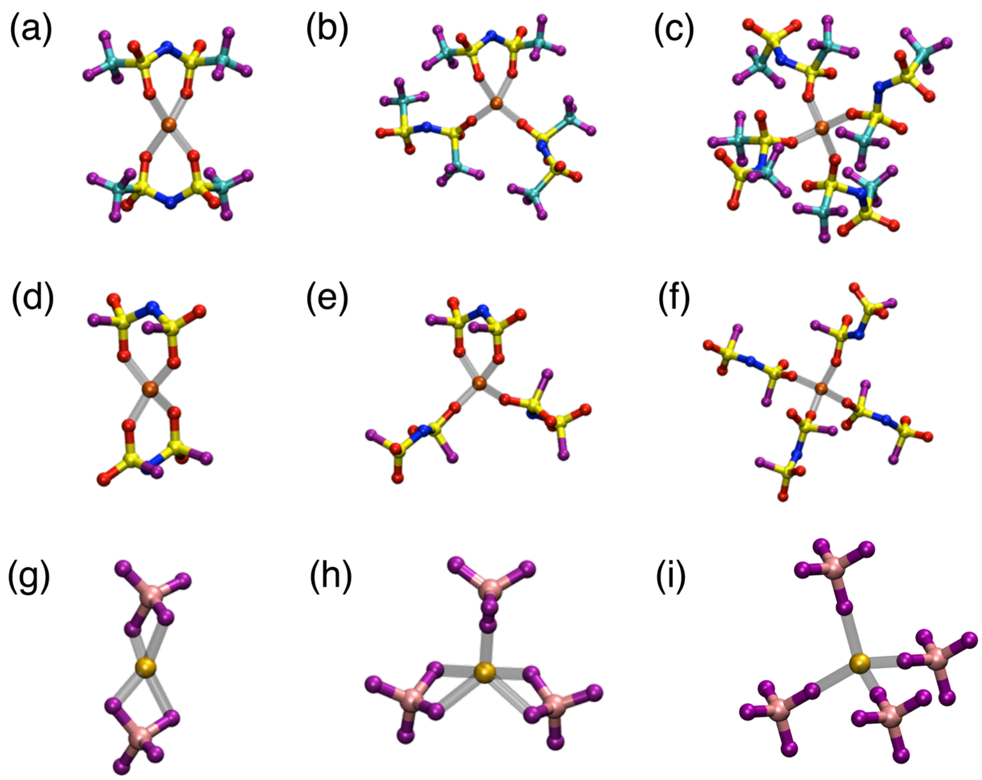

Figure 1. Energetically favorable $[Li(Anion)_n]^{(n-1)-}$ clusters from B3LYP/6-31+G** computations. Displayed are clusters having (a, d, g) $n = 2$, (b, e, h) $n = 3$, and (c, f, i) $n = 4$ anions for (a–c) [TFSI], (d–f) [FSI], and (g–i) $[BF_4]$. From DFT-MD simulations of liquids, solvation shells corresponding to clusters (a), (b), (d), (e), and (i) are found to be stable at 363 K.

■ LI^+ SOLVATION STRUCTURE

DFT Cluster Computations. To initiate our study of Li^+ solvation by ionic liquid, we have probed the configuration space of $[Li(Anion)_n]^{(n-1)-}$ clusters, with the number of anions, n, being varied from one to four, with DFT computations at the B3LYP/6-31+G** level. As previous theoretical and experimental[9,10,12,27,61−65] studies have suggested the number of Li-solvating anions for the liquids of interest here to be $2 \leq n \leq 4$, we herein limit our analysis to clusters with $n \leq 4$. In a previous work, we have found that in $Li[BF_4]$ clusters with $n = 2$ or 3, η^2 bonding dominates and produces the most energetically stable clusters at $T = 0$.[41] Upon reaching clusters with $n = 4$, the energy of bringing an anion close enough to form a η^2 bond is outweighed by the mutual anion−anion repulsion, which results in a stable $4\eta^1$ cluster. With this change in structure with coordination number in mind, we have extended our previous work to include $n = 2$, 3, and 4 clusters with both the *cis* and *trans* conformers of the [TFSI] and [FSI] anions, the results of which, along with $[BF_4]$, are summarized in Table 1, with the structures associated with the most energetically favorable clusters shown in Figure 1. To simplify the following discussion, we note distinct trends in the conformational preference of a given [TFSI] or [FSI] anion in a given cluster with Li-binding. It was found from using different combinations of conformers that $n \geq 2$ clusters having *trans*-[TFSI] are the most energetically stable, whereas [FSI] is more complex, with η^2 anions taking the *cis* conformation and η^1 anions taking the *trans* conformation. Only the low-energy clusters following these rules are shown in Table 1.

To elaborate upon the energetics of the clusters, we have decomposed the energy into the primarily repulsive interactions of the anions (E_R), which is the energy of bringing the anions into their cluster configuration from infinite separation without Li^+; the primarily attractive interaction between the Li^+ and the anions (E_A), which is obtained from the difference in total energy and E_R; and the cluster binding energy (E_B), where E_B =

DOI: 10.1021/acs.jpcb.5b06951
J. Phys. Chem. B 2015, 119, 14705−14719

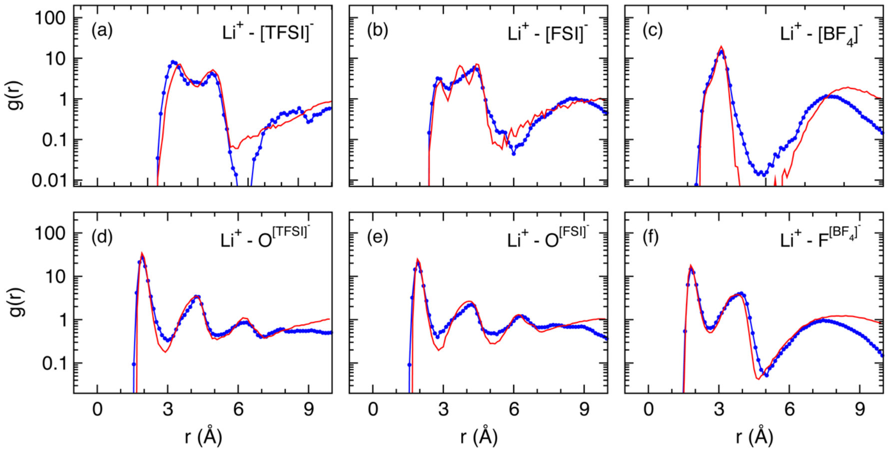

Figure 2. Radial distribution function ($g(r)$) as obtained by PFF-MD and DFT-MD simulation at T = 363 K for Li^+ with the ionic liquid anions (a) [TFSI], (b) [FSI], and (c) $[BF_4]$ as well as with the (d) O atoms in [TFSI], O atoms in [FSI], and F atoms in $[BF_4]$. The radial distributions are averaged over a 100 ps DFT-MD trajectory and a 6 ns PFF-MD trajectory, with one Li^+ in ionic liquid systems having 8, 10, and 12 pairs for [pyr14][TFSI], [pyr13][FSI], and $[EMIM][BF_4]$, respectively.

$-(E_R + E_A)$. In agreement with previous computations,[9,10,12,41] the n = 2 clusters assume η^2 configurations, whereas the n = 4 clusters assume η^1 configurations. For the n = 3 clusters, all anions evaluated exhibit more negative values of E_A with an increased number of η^2 configurations. In fact, as can be seen from Table 1, the conversion of any η^1 anion to an η^2 state decreases E_A by roughly 8−12 kcal/mol across all anions investigated. On the contrary, E_R exhibits the inverse relationship, with more η^2 binding leading to higher levels of repulsion, which is on the order of 8−11 kcal/mol for each η^1 anion converted to an η^2 state. For n = 3 clusters with [TFSI] and [FSI] anions, these energetic contributions appear to provide a minimum E_B in the $\eta^2 2\eta^1$ cluster, being 4.3 and 2.7 kcal/mol lower in energy than the fully bidentate $3\eta^2$ state in [TFSI] and [FSI], respectively. A comparative analysis of E_B between clusters with different values of n is difficult, as higher values of n necessarily lead to lower values of E_B due to increased anion repulsion. Solvation effects in a charge neutral system must be considered to provide more clarity on the relative stability of the Li^+ solvation shell with respect to n.

DFT-MD Liquid Simulations. A natural extension of the $[Li(Anion)_n]^{(n-1)-}$ cluster study is to introduce both temperature effects and solvation effects, which we accomplish here by performing liquid-phase DFT-MD simulations of our electrolytes in the presence of Li^+. To do this, for all three ionic liquids we have employed PFF-MD simulations to generate small, liquid-phase simulation cells having 8, 10, 12, and 16 pairs, with one cation in each system being replaced by Li^+. The structures are initially equilibrated using PFF-MD at 363 K for 10 ns, and multiple configurations of Li^+ having n = 2, 3, and 4 solvation shells are chosen as starting states for DFT-MD simulation. We perform 20 ps DFT-MD simulations with the system sizes and configurations so described, and we find that for the elevated T = 363 K simulation temperature is sufficiently long to sample multiple solvation shell configurations.

For [pyr14][TFSI] and [pyr13][FSI], we find n = 2 and 3 solvation structures, as shown in Figure 1a,b,d,e, to be stable over the 20 ps DFT-MD simulations, with the n = 4 solvation shells rapidly converting to an n = 3 state. Moreover, we find that the preferred n = 3 solvation shell corresponds to the most stable $\eta^2 2\eta^1$ cluster as evaluated from Table 1. On the contrary, the solvation shell of Li^+ in $[EMIM][BF_4]$ is primarily $4\eta^1$, as shown in Figure 1f, with the solvation shell transitionally assuming the $\eta^2 2\eta^1$ configuration, which agrees with the energetic trends noted in Table 1. From the present set of simulations, we have not observed strong size-related effects on the solvation shell; our smallest systems produce the same combination of solvation shells as our largest. These results are also in generally good agreement with the experimentally supported n = 2 [TFSI][10,64] and n = 3 [FSI].[12] However, the n = 3, [TFSI]-coordinated solvation structure has not heretofore been described by experiment. We suggest that such a structure is viable, and this will be additionally supported through a later comparison of computational and experimental Raman spectra.

Expanding on our DFT-MD study, we have benchmarked the structural similarity of PFF-MD simulations to that of the DFT-MD simulations. To improve the statistics of our first-principles molecular dynamics, we have performed an additional set of 100 ps DFT-MD simulations at 363 K beyond the initial 20 ps equilibration on the 8, 10, and 12 pair systems of [pyr14][TFSI], [pyr13][FSI], and $[EMIM][BF_4]$, respectively, which represent the largest systems that can be reasonably simulated with DFT-MD at such a time scale. Throughout these long simulations, no new solvation structures were observed. In Figure 2, we compare the radial distribution functions of these systems as obtained with DFT-MD to those produced from PFF-MD simulations at the same size and temperature conditions. Across the board, the agreement between the radial distribution functions is excellent, especially when the smaller, 100 ps length of the DFT-MD simulations is considered as compared to the 6 ns used for the PFF-MD simulations. In the [pyr14][TFSI] and [pyr13][FSI] cases, the initial $g(r)$ peak centered about r = 3 Å shows a double hump that is characteristic of the more distant η^1 anions and the closer η^2 anions. For $[BF_4]$, there is a much more localized signature around 3 Å, which encompasses both η^1 anions and the rarer η^2 anions. As signified by the agreement in both the shape and magnitude of the first $g(r)$ peak, the solvation structures observed from the PFF-MD simulations are very similar to those seen in DFT-MD. However, these results also suggest that PFF-MD slightly underpredicts the net amount of η^2 binding compared with the DFT-MD simulations, especially for [TFSI] and [FSI] anions.

DOI: 10.1021/acs.jpcb.5b06951
J. Phys. Chem. B 2015, 119, 14705−14719

PFF-MD Network Analysis. Although the previous analysis has been performed for the low Li-salt doping regime, we now discuss the case of high Li-salt doping and the potential influence of Li-networks on the experimental estimation of n. As Li-salt doping increases, the experimentally derived solvation number exhibits a marked decrease, with [TFSI]-based liquids decreasing to roughly $n = 1.5$ at $x_{\mathrm{Li}} > 0.15$.[9] Such a decrease cannot be attributed to the solvation numbers of individual Li^+, where coordination by one anion is not observed and must be related to the effect of Li-networks, where multiple Li^+ are bridged by mutual anions. Because current experimental practices can only determine total number of anions bound to all Li^+, the formation of networks, where a given anion can belong the solvation shell of multiple Li^+, leads to an underestimation of n. To quantify this effect, we have performed 216 ionic liquid pair room-temperature PFF-MD simulations having x_{Li} values of 0.05, 0.15, and 0.33 and have computed the average size of Li···Li network, $N_{\mathrm{Li\cdots Li}}$, the average number of anions in each individual Li^+ solvation shell, $\langle n \rangle$, and the total number of unique anions solvating all Li^+, $\langle N_s^- \rangle$, divided by the total number of Li^+, N_{Li}. The value of $\langle N_s^- \rangle / N_{\mathrm{Li}}$ is more aligned with that obtained from spectroscopic studies and is independent of the local solvation number of each anion, which simulation suggests to alway be 2 or 3. As shown in Table 2, the value of $N_{\mathrm{Li\cdots Li}}$ increases from 1.1 to 1.2 at $x_{\mathrm{Li}} = 0.05$ to 1.5−1.7 at $x_{\mathrm{Li}} = 0.33$, indicating a shift from isolated Li-ions at low Li-doping levels to Li-networks at moderate to high Li-doping levels. Furthermore, we note an inverse relationship between $\langle n \rangle$ and $\langle N_s^- \rangle / N_{\mathrm{Li}}$ with increasing x_{Li}; from $x_{\mathrm{Li}} = 0.05$ to $x_{\mathrm{Li}} = 0.33$, we see a slight increase of 0.1−0.3 in $\langle n \rangle$, while $\langle N_s^- \rangle / N_{\mathrm{Li}}$ is decreased by 1. The magnitude of Li-networking is notable in even the $x_{\mathrm{Li}} = 0.15$ system, where $\langle N_s^- \rangle / N_{\mathrm{Li}}$ decreases by a half. These results are in generally good agreement with experiment and suggest an underprediction of n at high x_{Li}; however, clarifying the exact magnitude of this effect would require a more quantitative look at the structure and vibrational frequencies of Li-networks, which is out of the scope of the present work.

Table 2. Room-Temperature Measures of the Average Li^+ Network Size, $\langle N_{\mathrm{Li\cdots Li}} \rangle$, the Average Number of Anions in the Solvation Shell of a Given Li^+, $\langle n \rangle$, and the Total Number of Unique Anions Solvating All Li^+, $\langle N_s^- \rangle$, Normalized by the Total Number of Li-Ions, N_{Li}, As Taken from PFF-MD Simulation with 144−216 Ion Pairs

	x_{Li}	$\langle N_{\mathrm{Li\cdots Li}} \rangle$	$\langle n \rangle$	$\langle N_s^- \rangle / N_{\mathrm{Li}}$
[pyr14][TFSI]	0.05	1.1	3.3	3.3
	0.15	1.4	3.3	2.8
	0.33	1.5	3.6	2.2
[pyr13][FSI]	0.05	1.1	3.8	3.7
	0.15	1.4	3.9	3.1
	0.33	1.6	4.0	2.5
[EMIM][BF_4]	0.05	1.2	3.9	3.7
	0.15	1.4	3.9	3.2
	0.33	1.7	4.0	2.6

■ VIBRATIONAL ANALYSIS OF LI^+ SOLVATION

Raman Analysis of Clusters. To experimentally corroborate our proposed Li^+ solvation shell structures, we now turn to a study of Raman spectroscopy. For [TFSI] and [FSI] anions, Raman spectroscopy allows the identification of characteristic anion vibrations that fundamentally change when bound to Li^+. By knowing the ratio of Li^+ to anions, we can directly relate the ratio of the magnitude of these modes to N_s^-, the total number of anions solvating all Li^+, as well as n, the characteristic number of anions in the solvation shell. With n at hand, the details of the solvation structure can be predicted through DFT cluster computations of Raman spectra. At room temperature and values of $x_{\mathrm{Li}} < 0.2$, such procedures have predicted Li^+ to be coordinated at room temperature by 1.86−2 [TFSI] anions in a $2\eta^2$ configuration[9−11] and 2.9−3 [FSI] anions in a $\eta^2 2\eta^1$ configuration, which reaches an equilibrium with an $n = 2$, $2\eta^2$ structure at higher temperature.[12] Although our previously discussed DFT/PFF-MD simulations do not dispute these results, we additionally find that $n = 3$ solvation structures are present in [pyr14][TFSI]. To explore the feasibility of this structure and assess the influence of structural variation on Raman activities, we presently re-evaluate the available experimental data by performing a thorough comparison of the DFT-mediated Raman spectra of $[\mathrm{Li(TFSI)}_n]^{(n-1)-}$ and $[\mathrm{Li(FSI)}_n]^{(n-1)-}$ clusters having $2 \le n \le 4$. Though the experimental findings have indeed also been aided by DFT Raman spectra,[9−12] we have here provided a more in-depth study on the influence of structure and value of n, especially for [TFSI] where $n = 3$ solvation structures have not been vibrationally characterized.

In [TFSI]-based ionic liquids, Li-salt doping gives rise to a new Raman signature between 745 and 750 cm^{-1}, which is a perturbation of the coupled CF_3 bend, $\delta_s(CF_3)$, and SN stretch, $\nu_s(SN)$, present at 742 cm^{-1} in neat samples. The experimental Raman spectra of these modes in neat [BMIM][TFSI] and [BMIM][TFSI] with $x_{\mathrm{Li}} = 0.33$ Li[TFSI], as taken from the work of Lasségues and co-workers,[9] is displayed in Figure 3d. As can be seen, when Li-salt doping levels increase, the higher-frequency signature from [TFSI] anions (the [BMIM] cations do not contribute significantly in this region) bound to Li^+ increases, while the lower-frequency signature, which is assumed to be entirely [TFSI] not bound to Li^+, decreases. Along with the reproduction of the experimental data in Figure 3, we have included our computed Raman activities for $[\mathrm{Li(TFSI)}_n]^{(n-1)-}$ clusters having n = 2, 3, and 4. The frequencies and activities shown were computed with B3LYP/6-31+G** for the $2\eta^2$ and $\eta^2 2\eta^1$ structures found from DFT-MD as well as the $4\eta^1$ structure that, though not observed through DFT-MD, has been previously proposed as a potential solvation structure. To provide a thorough estimate of Raman activities, we have additionally computed these structures in both their *cis* and *trans* conformations as well as with multiple local geometries, which in total lead to 2, 6, and 10 individual clusters computations for the $2\eta^2$, $\eta^2 2\eta^1$, and $4\eta^1$ clusters, respectively. As shown in Figure 3, $n = 2$ and $n = 3$ clusters have Raman active modes in the 745−755 cm^{-1} range, whereas $n = 4$ clusters appear to have modes shifted to lower frequencies in the 735−745 cm^{-1} range. Although $n = 2$ has a strong activity only in the high-frequency region, the $n = 3$ clusters have activities divided between the low- and high-frequency regions. From further analysis of our computed vibrational modes, it appears that primarily [TFSI] having η^2 binding appears in the high-frequency region, whereas η^1 is indistinguishable from the neat frequency. Therefore, given that experimental analysis associates 1.8−2 anions per Li^+ as coming from the 745−750 cm^{-1} signature, a potential scenario is a coexistence of $n = 2$ and $n = 3$ clusters.

DOI: 10.1021/acs.jpcb.5b06951
J. Phys. Chem. B 2015, 119, 14705−14719

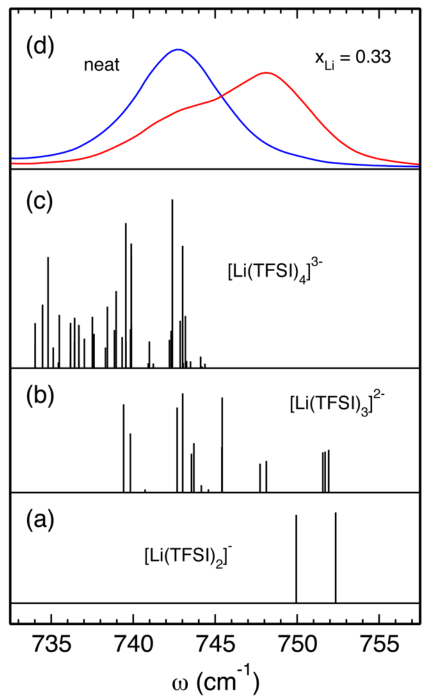

Figure 3. Raman active coupled CF_3 bend, $\delta_s(CF_3)$, SN stretch, ν_s(SN), modes of [TFSI] as determined by DFT for (a) n = 2, (b) n = 3, and (c) n = 4 $[Li(TFSI)_n]^{(n-1)-}$ clusters and (d) from the experiments of Lasségues and co-workers[9] for [BMIM][TFSI] in both the neat form and that having x_{Li} = 0.33 Li[TFSI]. A scaling factor of 0.987 was applied to our computational frequencies, which brings the $\delta_s(CF_3)$ stretch frequencies of isolated TFSI into agreement with the experimental measure from the neat ionic liquid.

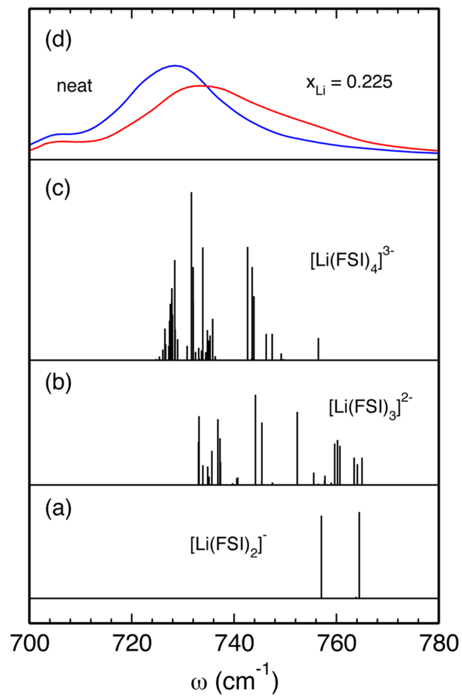

Figure 4. Raman active SN stretch, ν_s(SN), modes of [FSI] as determined by DFT for (a) n = 2, (b) n = 3, and (c) n = 4 $[Li(FSI)_n]^{(n-1)-}$ clusters and (d) from the experiments of Fujii and co-workers[12] for [EMIM][FSI] in both the neat form and that having x_{Li} = 0.225 Li[FSI]. A scaling factor of 0.963 was applied to our computational frequencies, which brings the ν_s(SN) stretch frequencies of isolated FSI into agreement with the experimental measure from the neat ionic liquid.

A similar Raman analysis can be performed for [FSI], in which both the ν_s(SN) at 731 cm^{-1} and the ν_s(SO) at 1220 cm^{-1} exhibit a strong dependence on Li-salt doping. As with [TFSI]-based ionic liquids, increasing the Li-salt doping in an [FSI]-based liquid results in a higher-frequency emission, which occurs at 744 cm^{-1} for the ν_s(SN) vibration and 1230 for the ν_s(SO) vibration, associated with anions bound to Li^+ progressively overtaking the lower-frequency emission of the free [FSI]. Experimental Raman spectra displaying the ν_s(SN) and ν_s(SO) Raman-active modes of [FSI] (the [EMIM] cations do not contribute significantly in this region), as taken from Fujii and co-workers,[12] are shown in Figures 4d and 5d, respectively, for [EMIM][FSI] in both the neat form and that having x_{Li} = 0.225 Li[FSI]. The associated DFT-derived Raman activities in these regions are included in Figures 4 and 5 for n = 2, 3, and 4 clusters. Similarly to the case of [TFSI] clusters, we have performed computations on clusters with *cis* and *trans* conformers as well as with multiple local geometries, again leading to 2, 6, and 10 individual clusters computations for the $2\eta^2$, $\eta^2 2\eta^1$, and $4\eta^1$ clusters, respectively. Concerning the ν_s(SN) vibrations, [FSI] associated with n = 4 clusters has Raman-active modes primarily appearing in the neat region, whereas [FSI] associated with n = 2 and 3 clusters has higher-frequency Raman active modes. For the ν_s(SO) mode, we see a slightly different behavior, with n = 3 and 4 clusters having activities arising in the high-frequency region and n = 2 clusters having activities appearing in the low-frequency region. In contrast to [TFSI], some $\eta^1\nu_s$(SN) vibrations in [FSI] appear in the high-frequency regions, which leads to n = 3 clusters having frequencies spanning a large region between 730 and 770 cm^{-1}. These activities are, however, roughly centered around 744 cm^{-1}, which corresponds to the experimental Raman-active frequency of [FSI] bound to Li^+. The ν_s(SO) mode of [FSI] appears to be more affected by Li-binding as most configurations of n = 3 and 4 clusters have strong activities in the high-frequency regions, with the exception of n = 2 clusters that, anomalously, appear at low frequency. Taking this with the experimental, room-temperature coordination of 2.9−3, we must conclude that n = 3 clusters are indeed dominant, and further, at high temperatures, where the coordination number via the ν_s(SO) mode is found to decrease to 2.5, the loss of activity in the high-frequency region can ascribed to the evolution of more n = 2 clusters.

IR Spectra of the Liquid Phase. Whereas the previous discussion of Raman spectra focused on how Li^+ alters the native vibrations of anions in its solvation shell, we now turn to a brief discussion of the spectroscopic signature that arises from the vibration of Li^+ itself. Such vibrations are most apparent at lower frequencies (<500 cm^{-1}) from IR spectroscopy, where IR active modes arise due to the vibration of Li^+ within its solvation shell, or the so-called "rattling" motions. In this respect, an interesting approach to characterizing the Li^+ IR signature is to leverage our long DFT-MD simulations at 363 K to compute the IR spectra. IR spectra computations from MD simulations are not commonly undertaken because the DFT-MD simulation time required to accurately resolve a frequency can be large for low-frequency vibrations, and classical MD simulations are generally not sufficiently accurate to produce viable spectra. However, the Li^+ rattling motions produce a broad IR signature that can be qualitatively characterized over

DOI: 10.1021/acs.jpcb.5b06951
J. Phys. Chem. B 2015, 119, 14705−14719

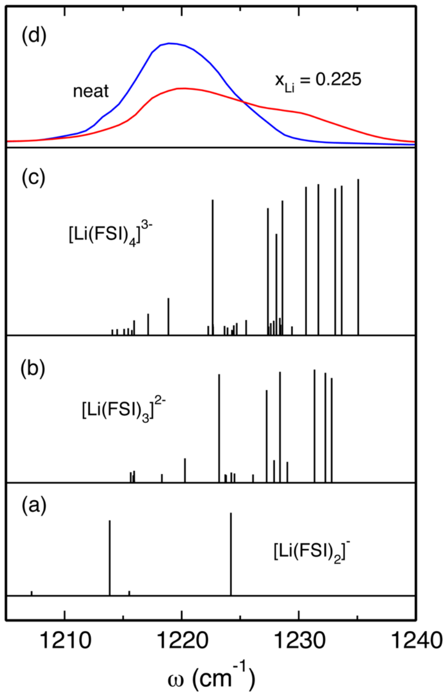

Figure 5. Raman active SO stretch, ν_s(SO), modes of [FSI] as determined by DFT for (a) n = 2, (b) n = 3, and (c) n = 4 $[Li(FSI)_n]^{(n-1)-}$ clusters and (d) from the experiments of Fujii and co-workers[12] for [EMIM][FSI] in both the neat form and that having x_{Li} = 0.225 Li[FSI]. A scaling factor of 1.054 was applied to our computational frequencies, which brings the ν_s(SO) stretch frequencies of isolated FSI into agreement with the experimental measure from the neat ionic liquid.

the 100 ps time scale of our DFT-MD simulations. To do this, we first characterize multiple configurations from our DFT-MD simulations with Bader analysis to obtain an approximate, average charge for each atomic species. The net charge so obtained can then be coupled with velocity data from the DFT-MD trajectory and used in an autocorrelation function, J,

$$J(t) = \langle \mathbf{M}(t)\cdot\mathbf{M}(0)\rangle \quad (1)$$

where $\mathbf{M}(t) = \sum_{i=0}^{i=N} q_i \mathbf{v}_i(t)$. By simply taking the Fourier transform of $J(t)$, one can then obtain the temperature-dependent IR spectrum of a given system, $\tilde{J}(\omega)$.

The results of our DFT-MD procedure for our three ionic liquids are shown in Figure 6 and compared with the IR signature of the Li^+ vibrations obtained using DFT and the harmonic frequencies of all the clusters investigated in this work. For the most part, the spectra computed from DFT-MD simulation are in qualitatively good agreement with the IR spectra produced from cluster simulations. The Li^+ IR active modes, which are independent of ionic liquid, are broadly spread about 300 cm^{-1}, which is in good agreement with experimental measures having a broad absorption around 374 cm^{-1}.[9] Interestingly, the IR signatures of the modes appear in the same frequency region for all three ionic liquids, which suggests the curvatures of the Li-binding are similar in spite of the different preferred solvation shells and anions. We also note that the temperature-induced broadening from our DFT-MD simulations is well-approximated by the use of many clusters having different conformations, which, along with the previously described Raman study of cluster coordination number, suggests that multiple configurations of solvation

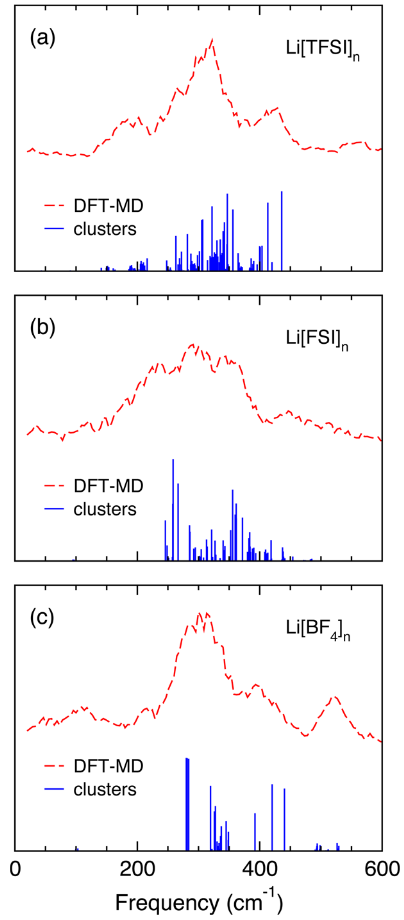

Figure 6. Infrared signature of Li^+ in (a) [pyr14][TFSI], (b) [pyr13][FSI], and (c) [EMIM][BF_4] as obtained from both 100 ps DFT-MD simulations at T = 363 K and DFT computations of the geometry optimized $[Li(Anion)_n]^{(n-1)-}$ clusters presented in Table 1. The intensities of the DFT-MD spectra are shifted upward for ease of comparison with cluster results.

complexes are required to obtain a reasonable measure of IR absorption or Raman activity.

■ TRANSPORT PROPERTIES

We now turn to an investigation of transport from our 100 ps DFT-MD liquid simulations of 7[pyr14][TFSI] + Li[TFSI], 9[pyr13][FSI] + Li[FSI], and 11[EMIM][BF_4] + Li[BF_4]. With regard to ion transport, PFF-MD using APPLE&P has proven an invaluable tool, with computed transport coefficients for ionic systems, which are traditionally inaccurate from classical MD simulations, being in close agreement with experimental measurements.[17,26,31,33] As an alternative to PFF-MD, one may employ DFT-MD simulations[34,35] in the liquid phase and determine the transport coefficients from the resulting trajectory data. However, due to the extraordinarily large computational cost of DFT-MD, there will ultimately be limitations on both the simulation size and the simulation duration, both of which strongly play into the statistical accuracy of the diffusion coefficient. To this end, we here benchmark the potential system size and simulation time effects present in our DFT-MD simulations through the analysis of trends in equivalently sized PFF-MD simulations. As a means of understanding the simulation time influence on our DFT-MD simulations, we compare the apparent diffusion coefficients

DOI: 10.1021/acs.jpcb.5b06951
J. Phys. Chem. B 2015, 119, 14705−14719

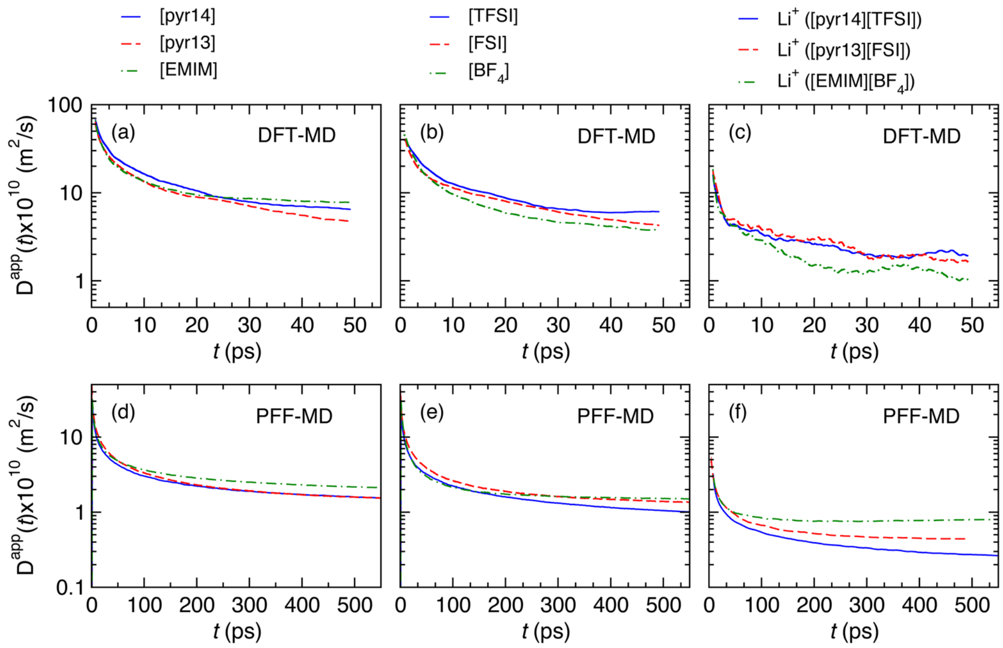

Figure 7. Apparent diffusion coefficient of ($D^{\mathrm{app}}(t)$) as a function of time from (a−c) DFT-MD and (d−f) PFF-MD simulation at T = 363 K using small cells having 8, 10, and 12 pairs of [pyr14][TFSI], [pyr13][FSI], and [EMIM][BF$_4$], respectively, with one cation replaced by Li$^+$. The values of D^{app} as given are representative of many time-origin averages, N^{o}, for both the 100 ps DFT-MD simulations (N^{o} = 20) and the 6 ns PFF-MD simulations (N^{o} = 300).

Table 3. Values of $D^{\mathrm{app}}(t)$ (in Units of 10^{-10} m^2/s) for Ions in Ionic Liquids at 363 K As Evaluated Using Both DFT-MD and PFF-MD[a]

		t^{sim}	N_{pairs}	t	$D^{+,\mathrm{app}}(t)$	$D^{-,\mathrm{app}}(t)$	$D^{\mathrm{Li,app}}(t)$
[pyr14][TFSI]	DFT-MD	0.1	8	0.05	6.47 (3.2)	6.10 (2.4)	1.91 (0.6)
	PFF-MD	6.0	8	0.05	4.23	3.17	0.75
		6.0	8	$t \to \infty$	1.40	0.89	0.28
		6.0	144	$t \to \infty$	0.80	0.66	0.34
[pyr13][FSI]	DFT-MD	0.1	8	0.05	4.78 (2.3)	4.27 (2.4)	1.64 (0.5)
	PFF-MD	6.0	8	0.05	4.85	3.85	0.92
		6.0	8	$t \to \infty$	1.41	1.29	0.44
		6.0	216	$t \to \infty$	0.89	0.91	0.47
[EMIM][BF$_4$]	DFT-MD	0.1	8	0.05	7.77 (3.6)	3.78 (2.2)	1.03 (0.3)
	PFF-MD	6.0	8	0.05	4.77	2.97	0.97
		6.0	8	$t \to \infty$	1.97	1.48	0.75
		6.0	216	$t \to \infty$	1.93	1.38	0.65

[a]The total MD simulation length (t^{sim}) in picoseconds, the number of ion pairs in the MD simulation (N_{pairs}), and the time (t) used to evaluate $D^{\mathrm{app}}(t)$ in picoseconds is given for each system. Values for the largest 144−216 N_{pairs} PFF-MD systems are interpolated to the DFT-MD x_{Li} values from independent simulations of x_{Li} = 0.05, 0.10, and 0.15. Error as obtained from the standard deviation of the N^{o} time origins used to average $D^{\mathrm{app}}(t)$ is given for the DFT-MD results in parentheses.

(given as $D^{\mathrm{app}}(t)$, where t is time) of cations, anions, and Li$^+$ obtained from both our DFT and PFF simulations. The $D^{\mathrm{app}}(t)$ values are a convenient means of understanding how error in the diffusion coefficient changes with simulation time, with the thermodynamic diffusion coefficient (D) being equal to the long time limit of the apparent diffusion coefficient, $D^{\alpha} = \lim_{t\to\infty} D^{\alpha,\mathrm{app}}(t)$, where α is a particular ionic species. Both coefficients are, of course, related to the mean square displacement of the ionic species,

$$D^{\alpha} = \lim_{t\to\infty} \frac{1}{6t} \sum_{i=1}^{N^{\alpha}} \sum_{j=1}^{N^{\mathrm{o}}} \langle [\mathbf{r}^{\alpha,i}(t-t_j) - \mathbf{r}^{\alpha,i}(t_j)]^2 \rangle / (N^{\alpha} N^{\mathrm{o}}) \quad (2)$$

where $\mathbf{r}^{\alpha,i}$ is the atomic position of one of the N^{α} atoms in molecular species α and t_j is the jth time origin, with the diffusion being an average over N^{o} time origins.

In Figure 7, we present measures of $D^{\mathrm{app}}(t)$ as a function of time for the various species in the ionic liquids of interest at 363 K. For the DFT-MD measures, given in Figure 7a−c, the total simulation times are 100 ps total simulation time, N^{o} is taken as 20, and the apparent diffusion coefficient is shown up to t = 50 ps, which results in generally well-behaved $D^{\mathrm{app}}(t)$ profiles. We note that diffusion within the relatively short 50 ps time scale appears to still be within the ballistic regime; that is, the apparent diffusion is still correlated to its previous states and provides an overestimate of thermodynamic diffusion, with the thermodynamic limit being expected at large values of t where $D^{\mathrm{app}}(t)$ is constant. Despite this overestimate, the values of

DOI: 10.1021/acs.jpcb.5b06951
J. Phys. Chem. B 2015, 119, 14705−14719

Table 4. Various DFT Measures of the Difference between the Ionization Energy of Anions (IE) and Electron Affinity of Cations (EA) for Adiabatic ($\Delta E_{IE,a}$) and Vertical ($\Delta E_{IE,v}$) Excitations (Simulations Performed on Isolated Ions)[a]

		BPW91	PW91	PBE	HSE06	B3LYP	M06
[pyr14][TFSI]	EA_a	2.448	2.624	2.594	2.387	2.468	2.473
	IE_a	5.138	5.238	5.153	5.438	5.450	5.490
	$\Delta E_{IE,a}$	2.690	2.613	2.559	3.050	2.982	3.018
	EA_v	2.425	2.604	2.574	2.372	2.455	2.458
	IP_v	5.784	5.867	5.782	6.350	6.344	6.352
	$\Delta E_{IE,v}$	3.359	3.263	3.208	3.978	3.889	3.894
[pyr13][FSI]	EA_a	2.467	2.646	2.615	2.408	2.492	2.496
	IE_a	5.138	5.442	5.361	5.603	5.653	5.663
	$\Delta E_{IE,a}$	2.671	2.796	2.746	3.195	3.161	3.167
	EA_v	2.445	2.626	2.597	2.394	2.479	2.483
	IE_v	6.069	6.148	6.064	6.604	6.607	6.594
	$\Delta E_{IE,v}$	3.624	3.521	3.468	4.210	4.128	4.111
[EMIM][BF_4]	EA_a	3.803	3.890	3.836	3.805	3.860	3.869
	IE_a	6.460	6.558	6.462	6.956	7.035	7.035
	$\Delta E_{IE,a}$	2.657	2.668	2.626	3.150	3.175	3.166
	EA_v	3.207	3.323	3.267	3.167	3.220	3.211
	IE_v	6.508	6.607	6.510	7.448	7.360	7.367
	$\Delta E_{IE,v}$	3.301	3.284	3.242	4.281	4.140	4.156

[a]The 6-31+G** basis set is used across all levels of theory, and the units are electronvolts.

$D^{app}(t{=}50\ ps)$ are the correct order of magnitude when compared to experimental[15−17] and previous computational[26] measures of diffusion and further follow the trend where the diffusion of cations (D^+) > anions (D^-) > Li^+ (D^{Li}). The values of $D^{app}(t)$ from PFF-MD using simulation cells equivalent to those of DFT-MD, as shown in Figure 7d−f, are well-converged and smooth, with the total simulation time being 6 ns, N^o being 300, and the apparent diffusion being shown up to t = 500 ps. These, too, follow the trend of $D^+ > D^- > D^{Li}$ and agree in magnitude with the DFT-MD results. The much longer time scales in PFF-MD simulations reveal that the ballistic regime is long-lived and on the order of hundreds of picoseconds.

For a more quantitative comparison of the diffusion estimates, we provide in Table 3 measures of $D^{app}(t)$ as obtained from small DFT-MD and PFF-MD simulation cells at t = 50 ps and for small and large PFF-MD simulation cells in the thermodynamic limit, given as $t \to \infty$. First, comparing small PFF-MD and DFT-MD cells, we note that with only a few exceptions the DFT-MD values of $D^{app}(t{=}50\ ps)$ are somewhat larger than those produced by PFF-MD; however, considering the error in the DFT-MD estimates, which is ~50% for the cations and anions and ~30% for the Li^+ ions, most of the PFF-MD results are within the error bars of the DFT-MD. To elaborate upon the diffusion of Li^+ in particular, we note the ratio of $D^{Li,app}(t\to\infty)$ to $D^{Li,app}(t{=}50\ ps)$ for the small PFF-MD systems is 0.37, 0.48, and 0.77 for [pyr14][TFSI], [pyr13]-[FSI], and [EMIM][BF_4], respectively. Assuming the DFT-MD simulations would exhibit a similar decrease as $t \to \infty$ leads to Li^+ diffusion values of 0.71×10^{-10}, 0.78×10^{-10}, and 0.8×10^{-10} m^2/s, for [pyr14][TFSI], [pyr13][FSI], and [EMIM-BF_4], respectively. This is in good agreement with available experimental measurements (extrapolated to 363 K) for [pyr14][TFSI],[15,17] which range from 0.85×10^{-10} to 1.91×10^{-10} m^2/s, and for [EMIM][BF_4],[16] which is estimated to be 0.8×10^{-10} m^2/s, whereas the lack of experimental data for [pyr13][FSI] makes a meaningful comparison difficult.

To quantify potential size effects related to the small-cell DFT-MD and PFF-MD results, we compare our small PFF-MD results to previously reported diffusion coefficients[26] as computed from PFF-MD simulations having 144 ion pairs for [pyr14][TFSI] and 216 ion pairs for both [pyr13][FSI] and [EMIM][BF_4]. To maintain a uniform value of x_{Li} across simulation size, we interpolate our large cell diffusion coefficient to the appropriate small cell value of x_{Li} from values taken from independent simulations at 0.05, 0.10, and 0.15. Interestingly, we note that as system size is increased, we generally see a decrease in D^+ and D^-. On the basis of their radial distribution functions, the cations and anions in the [pyr14][TFSI] and [pyr13][FSI] small cell systems are solvated by roughly 0.7−0.8 fewer counterions than those in large cells. This phenomenon is less pronounced in [EMIM]-[BF_4], where the small ion size and relatively larger number of pairs in the small cell lead to only 0.2 fewer solvating counterions than in the large cells. We therefore attribute the larger diffusion of cations and anions in small cells to an incomplete solvation structure that results in lower activation barriers to diffusion processes. This effect is smaller in small cell [EMIM][BF_4] as the ion species have a solvation structure more akin to that of large cells.

For Li^+, however, the correlation between cell size and diffusion is more complex, with D^{Li} increasing with increasing cell size in the [pyr14][TFSI] and [pyr13][FSI] systems and decreasing in the [EMIM][BF_4] system. As shown in a previous work,[26] Li^+ diffusion is influenced by anion exchange (Li^+ exchanges solvating anions with surrounding ionic liquid) and Li-network formation (the solvation shells of multiple Li^+ share anions). In large cells, the anion exchange rate for the ionic

DOI: 10.1021/acs.jpcb.5b06951
J. Phys. Chem. B 2015, 119, 14705−14719

Table 5. Various DFT Measures of the Difference between the LUMO and HOMO Energies (ΔE_{HL}) and between the Ionization Energy (IE) and Electron Affinity (EA) for Adiabatic ($\Delta E_{IE,a}$) and Vertical ($\Delta E_{IE,v}$) Excitations of Ion Pairs (Simulations Performed on an Interacting Cation/Anion Pair)[a]

		BPW91	PW91	PBE	HSE06	B3LYP	M06
[pyr14][TFSI]	ΔE_{HL}	4.993	4.781	4.823	6.267	6.390	6.340
	EA_a	0.052	0.168	0.134	−0.017	0.064	−0.189
	IE_a	7.882	8.141	8.055	8.442	8.373	8.875
	$\Delta E_{IE,a}$	7.830	7.973	7.921	8.459	8.309	9.064
	EA_v	−0.011	0.117	0.081	−0.065	0.014	−0.247
	IE_v	8.719	8.862	8.779	9.437	9.356	9.663
	$\Delta E_{IE,v}$	8.730	8.745	8.698	9.502	9.342	9.910
[pyr13][FSI]	ΔE_{HL}	5.085	4.823	4.859	6.364	6.475	6.479
	EA_a	2.150	1.185	1.078	0.008	0.099	−0.183
	IE_a	8.178	8.369	8.288	8.611	8.569	8.921
	$\Delta E_{IE,a}$	6.028	7.184	7.210	8.603	8.470	9.104
	EA_v	0.009	0.177	0.136	−0.045	0.039	−0.232
	IE_v	9.109	9.228	9.148	9.726	9.660	9.977
	$\Delta E_{IE,v}$	9.100	9.051	9.012	9.771	9.621	10.209
[EMIM][BF_4]	ΔE_{HL}	4.549	4.797	4.660	6.561	6.841	6.900
	EA_a	0.481	0.436	0.426	0.338	0.452	0.243
	IE_a	8.284	8.504	8.423	8.555	8.608	8.640
	$\Delta E_{IE,a}$	7.803	8.068	7.997	8.217	8.156	8.397
	EA_v	−0.096	−0.027	−0.058	−0.261	−0.164	−0.386
	IE_v	9.551	9.647	9.576	10.215	10.214	10.206
	$\Delta E_{IE,v}$	9.647	9.674	9.634	10.476	10.378	10.592

[a]The 6-31+G** basis set is used across all levels of theory, and the units are electronvolts.

liquids and conditions of interest ranges from 1 to 3.6 ns, and the percent of Li^+ participating in an Li-network ranges from 6 to 20%.[26] Anion exchange was further found to be beneficial to diffusion, whereas Li-network formation correlates the motion of multiple Li^+ and decreases diffusion. In small cells of [pyr14][TFSI] and [pyr13][FSI], the anion exchange rate is roughly a factor of 3 higher than that in large cells, likely because the surrounding liquid is not in its large cell configuration, and having a single Li^+, there are no networks. Barring other effects, this suggests that artificially high anion exchange rates suppress the diffusion coefficient, perhaps disrupting the vehicular mechanism (motion of Li^+ with its solvation shell) that was found to play a primary role in the diffusion of these systems in large cells.[26] Even given the suppressive effect of Li-networks on D^{Li}, the reduced exchange rate leads to a net higher measure of diffusion in large cells. Having a greater number of pairs, [EMIM][BF4] has a small cell anion exchange rate (1.2 ns) comparable with that of the large cell (1.6 ns). The primary remaining effect, then, is the formation of Li-networks, which leads to the noted decrease in diffusion in large cells.

Taken all together, the small-cell PFF-MD results are within 20−40% agreement with the large-cell results. For the time scales accessible to DFT-MD (~100 ps), the results suggest that the influence of simulation time, which can result in diffusion coefficients several times too large, is more important than simulation size, which results in 20−40% variance of diffusion coefficient. It is not clear, however, that the secondary influence of system size is a universality for all systems, with even previous MD simulations of other ionic liquids suggesting significant size effect up to many hundreds of pairs.[66]

■ ELECTROCHEMICAL STABILITY

Single Ions and Interacting Cation/Anion Pairs. As it currently stands, the majority of computational approaches for evaluating electrochemical windows are based on electronic energy levels of isolated or solvated electrolyte molecules.[21−23,25] Although more complex treatments exist,[20,24,40] we here follow and evaluate the validity of this convention on the basis of DFT-derived electronic energy levels.[21−23,25] For isolated electrolyte molecules, two natural measures of electrochemical stability are the energy difference between the LUMO and HOMO, ΔE_{HL}, and the difference between the IE and EA, given here as $\Delta E_{IE,a}$ for fully geometry relaxed, adiabatic measures and $\Delta E_{IE,v}$ for instantaneous, vertical measures. An extension of these procedures can be made to the liquid phase, where the difference between HOMO and LUMO energies in isolated electrolyte molecules can be equated to the difference between the CBM and VBM energies in periodic DFT simulations.

Table 4 displays estimates of electrochemical window on the basis of $\Delta E_{IE,a}$ and $\Delta E_{IE,v}$ for single, isolated ions, with EA being obtained from the cations and IE being obtained from the anions. For comparative purposes, we have presented results

DOI: 10.1021/acs.jpcb.5b06951
J. Phys. Chem. B 2015, 119, 14705−14719

from a wide range of pure exchange/correlation functionals, including BPW91, PW91, and PBE, as well as a variety of hybrid functionals, including HSE06, B3LYP, and M06, which are all evaluated with the 6-31+G** basis set. For measures of $\Delta E_{IE,a}$ and $\Delta E_{IE,v}$ hybrid functionals provide estimates 0.4−0.6 eV higher than the pure functionals. In all cases $\Delta E_{IE,a} < \Delta E_{IE,v}$, with the relaxation of the ions in the adiabatic case reducing the electrochemical window by 0.5−1 eV. Table 5 displays estimates of electrochemical window on the basis of ΔE_{HL}, $\Delta E_{IE,a}$, and $\Delta E_{IE,v}$ for an interacting cation/anion pair. Of interest, IE and EA computed from interacting ion pairs are larger and smaller, respectively, than those from isolated ions, which is a result of the electrostatic interaction that makes adding or removing an electron more difficult. This leads to the windows estimated from pairs being 5−6 eV higher than those from single ions. Similar to the case of single ions, for measures of $\Delta E_{IE,a}$ and $\Delta E_{IE,v}$ hybrid functionals are 0.5−1.0 eV higher than the pure functionals. Concerning ΔE_{HL}, there is a clear divide between the pure and hybrid functionals, with the hybrid functionals yielding 1.5−2 eV higher measures, in general agreement with the underestimation of the HOMO/LUMO gap in pure functionals. For almost all cases $\Delta E_{HL} < \Delta E_{IE,a} < \Delta E_{IE,v}$, with ΔE_{HL} being 3−4 eV lower than the measures from ionization energy and electron affinity; the exception to this is [pyr13][FSI] as treated with pure functionals, where the [FSI] decomposed in the adiabatic regime.

Among the three liquids, the values of $\Delta E_{IE,a}$ and $\Delta E_{IE,v}$ as obtained both from isolated ion computations and from interacting pairs show variations ≤1 eV. Further, the magnitudes of ΔE_{HL} among the three cation/anion pairs are similar, with the variation among the liquids for a given functional being <0.6 eV. The experimentally measured electrochemical windows are 3.8−6,[36,37,67] 5.3,[38] and 4.3 eV[68,69] for [pyr14][TFSI], [pyr13][FSI], and [EMIM][BF_4], respectively. Comparing our computations to experiment, we find that the IE-EA procedures on isolated ions and interacting cation/anion pairs provide a lower and upper bound, respectively, to the experimental data. This is reasonable as the two systems represent extremes of the solvation environment a molecule would feel in the liquid phase. Similarly, for the LUMO−HOMO procedure the pure functional provides a lower bound and the hybrid provides an upper bound to the experimental electrochemical window. The exception to this is [EMIM][BF_4], where ΔE_{HL} from pure functionals provides close agreement with experiment.

Liquid-Phase Simulations. Following the implication from the interacting cation/anion pair DFT computations that ΔE_{HL} is a straightforward means of bounding the electrochemical window, we now investigate the influence of temperature and solvation effects on these measures through coupled PFF-MD and DFT simulation. In this respect, we use PFF-MD as a platform for generating structures at room temperature and perform single point, DFT computations on select structures to generate an average measure of the difference between the CBM and VBM, given as ΔE_{VC}, which is akin to the value of ΔE_{HL} in isolated molecules. An alternative approach would be to employ the polarizable continuum medium approach on DFT simulations of single ionic liquid pairs. However, it has recently been shown that the quadrupolar interactions present in the liquid solvent surrounding a target solute are difficult to approximate with continuum models,[20] which, especially considering the ionic nature of our electrolyte, has led to our use of full liquid systems for the electrochemical window computations. As previously noted,[25] a serious concern with liquid-phase simulations is the influence of system size on the resulting ΔE_{VC}. To better understand potential size effects, we have performed PFF-MD simulations of liquid-phase systems having 12, 18, and 24 ionic liquid pairs, the simulation lengths of which are 60 ns at room temperature. From these simulations we have taken 10 representative snapshots, which are 6 ns apart to ensure that the structures are significantly different, and performed electronic structure computations with DFT using the pure functionals PBE and PW91 and the hybrid functionals HSE06 and B3LYP. The results, shown in Table 6, indicate that for all liquids there is a significant structural influence on the electronic energy levels, and thereby the estimate of electrochemical window, for systems composed of fewer than 18 ion pairs.

Table 6. Influence of the Number of Ionic Liquid Cation/Anions Pairs (N_{pairs}) on Liquid-Phase DFT Measures of the Difference between the Conduction Band Minimum (CBM) and Valence Band Maximum (VBM) Energies, Referred to as ΔE_{VC}[a]

		$4\Delta E_{VC}$			
	N_{pairs}	PW91	PBE	HSE06	B3LYP
[pyr14][TFSI]	1	4.78	4.82	6.27	6.39
	12	4.71	4.71	6.39	6.66
	18	4.58	4.58	6.25	6.51
	24	4.59	4.59	6.25	6.53
[pyr13][FSI]	1	4.82	4.86	6.36	6.48
	12	4.86	4.83	6.60	6.86
	18	4.74	4.71	6.46	6.73
	24	4.73	4.70	6.48	6.74
[EMIM][BF_4]	1	4.80	4.66	6.56	6.84
	12	4.00	4.01	5.21	5.96
	18	3.91	3.91	5.15	5.47
	24	3.92	3.92	5.15	5.46

[a]Energy is given in electronvolts. The N_{pairs} = 1 case is is reproduced from LUMO−HOMO values in Table 5.

Guided by our size effect study, we have made estimates of the electrochemical window of our electrolytes both in the neat form and with Li-salt doping. We have used our largest 24 ion pair system and replaced cations with Li^+ to achieve systems having x_{Li} values of $0.08\overline{3}$, $0.1\overline{66}$, 0.25, and $0.3\overline{33}$. For each system, we have employed the previously described procedure for generating 10 sample structures and evaluating the final value of ΔE_{VC} as an average over these structures, the results of which are displayed in Table 7.

For the neat ionic liquid systems reported in Table 6, we see that solvation has little effect on the measure of ΔE_{VC} as compared to ΔE_{HL} for [pyr14][TFSI] and [pyr13][FSI]. On the contrary, solvation systematically reduces the electrochemical window estimates for [EMIM][BF_4], which could be related to the greater degree of aromaticity in the [EMIM] cation as compared to [pyr14] and [pyr13]. In all cases, the liquid-phase computations result in the experimental electrochemical window being within the bound of the pure and hybrid functionals, including [EMIM][BF_4] in contrast to the cation/anion pair study. Additionally, the variation of ΔE_{VC} between the neat and Li-doped species suggest that the addition of Li^+ has little influence on this measure of electrochemical window, Table 7. For each system, the change

DOI: 10.1021/acs.jpcb.5b06951
J. Phys. Chem. B 2015, 119, 14705−14719

Table 7. Influence of Li-Salt Mole Fraction (x_{Li}) on the Difference in Conduction Band Minimum and Valence Band Maximum Energies (ΔE_{VC}) As Determined from Liquid-Phase DFT Simulations Having 24 Ion Pairs[a]

			ΔE_{VC}		
	x_{Li^+}	PBE	HSE06	B3LYP	exp
[pyr14][TFSI]	0.000	4.59	6.25	6.53	3.8–6[36,37,67]
	0.08$\overline{3}$	4.61	6.28	6.57	
	0.16$\overline{6}$	4.50	6.22	6.51	
	0.250	4.50	6.24	6.53	
	0.33$\overline{3}$	4.36	6.05	6.34	
[pyr13][FSI]	0.000	4.70	6.48	6.74	5.3[38]
	0.08$\overline{3}$	4.53	6.32	6.58	
	0.16$\overline{6}$	4.42	6.25	6.51	
	0.250	4.62	6.43	6.68	
	0.33$\overline{3}$	4.61	6.44	6.68	
[EMIM][BF_4]	0.000	3.92	5.15	5.46	4.3[68,69]
	0.08$\overline{3}$	3.97	5.22	5.53	
	0.16$\overline{6}$	4.07	5.30	5.61	
	0.250	4.09	5.31	5.47	
	0.33$\overline{3}$	3.96	5.18	5.50	

[a]Energies are given in units of electronvolts.

in electrochemical window with varying degrees of Li-salt doping is on the order of 0.2 eV, which is approximately the uncertainty of our measures of ΔE_{VC} (~0.2–0.3). Essentially, this suggests the chemical effect of Li-salt doping is low as the cations and Li^+ have a similar electrostatic influences on their surrounding solvent molecules.

CONCLUSIONS

The present work is an attempt to unite different levels of electronic and atomistic theory to provide an understanding of the physical properties of electrolytes for battery applications. We have combined zero-temperature DFT, DFT-MD, and PFF-MD to varying degrees to elucidate the structure, vibrations, transport, and electrochemical stability of three Li-doped ionic liquid electrolytes: [pyr14][TFSI], [pyr13][FSI], and [EMIM][BF_4].

Using a combination of DFT energetics of $[Li(Anion)_n]^{(n-1)-}$ and DFT-MD simulations of Li^+ in liquid-phase electrolyte, we have determined the number of anions, n, and preferred configuration of the Li^+ solvation shell at low Li-doping levels. Both [pyr14][TFSI] and [pyr13][FSI] exhibit Li^+ solvation structures that contain either two anions, both having bidentate ligand bonds, or three anions, one being bidentate and the other being monodentate, whereas [EMIM]-[BF_4] shows a tendency toward a solvation shell having four monodentate anions. The DFT cluster computations are found to successfully predict the most likely DFT-MD structures for a given value of n, and therefore represent a relatively inexpensive technique to survey likely solvation structures. They also allow a direct comparison of the Raman spectra of solvation structures to experimental measurements on Li-doped electrolytes. In this way, we find that our predicted solvation structure having two to three anions for [pyr14][TFSI] and [pyr13]-[FSI] (there is no available data for [EMIM][BF_4]) are consistent with experiment. To understand solvation structure at high Li-doping levels, we employ classical PFF-MD simulations with large systems. For $x_{Li} \geq 0.1$ we find that the low Li-doping solvation structures transition to highly coordinated Li-networks, where a single anion participates in multiple Li^+ solvation shells. The sharing of anions can consequently skew experimental measures of the number of anions in the Li+ solvation shell to lower values.

Combining DFT-MD and PFF-MD at 363 K, we have shown that DFT-MD is a viable technique for estimating the diffusion coefficient of Li^+. We obtain from 100 ps DFT-MD simulations diffusion coefficients of the electrolyte and Li^+ that are the same order of magnitude as, though an upper bound to, experimental measurements. To understand the origin of the error in our DFT-MD diffusion measurements, which can arise from the small simulation cells, 8–12 ionic liquid pairs, and short simulation duration, ~100 ps, we perform illustrative benchmarks with small and large simulations cells in PFF-MD. Using a small cell with PFF-MD, we find the diffusion at 100 ps is ballistic and an overestimate by a factor of 2–3 of the limit as $t \to \infty$. The PFF-MD diffusions in the $t \to \infty$ range (which is practically reached at $t > 2$ ns) in small cells and large cells are comparable and show a smaller 20–40% variance. This suggests the majority of the error in the DFT-MD diffusion coefficients arises from the short time scales used as opposed to the small size of the simulation cells. For Li^+ in particular, assuming the DFT-MD diffusion would show a similar decrease as noted in the PFF-MD simulations brings our DFT-MD measures into close agreement with experiment.

Finally, we have determined that DFT measures of differences between the lowest unoccupied and highest occupied electronic states and differences between the ionization energy and electron affinity may be a straightforward means of bounding the electrochemical window. Using DFT simulations, we find that IE-EA from single ions and interacting cation/anion pairs provide lower and upper bounds, respectively, to the experimental electrochemical window. Solvation effects on the molecular-level measurements are evaluated by generating liquid-phase configurations of ionic liquids with PFF-MD at 298 K and performing single-point DFT computations on these structures. This allows us to obtain a configurational average of the difference between the conduction band minimum and the valence band maximum energies. As with the molecular-level computations, liquid-phase measures from pure and hybrid functionals provide lower and upper bounds, respectively, to experiment. Further, solvation effects on the electrochemical window, as evaluated through these coupled DFT/PFF-MD simulations, change the electrochemical window by only 5–10%, except for the case of [EMIM][BF_4], which exhibits a 20–25% change in electrochemical stability upon solvation. To understand the potential influence of Li^+ on the electrochemical window, we apply the same coupled procedure to ionic liquid systems with $0.083 \leq x_{Li} \leq 0.33$. The effect of Li-salt doping on electrochemical window appears to be minor across the board, with all Li-doped systems providing electrochemical window measures within the error bars of the neat value.

AUTHOR INFORMATION

Corresponding Author

*J. W. Lawson. E-mail: john.w.lawson@nasa.gov.

Notes

The authors declare no competing financial interest.

ACKNOWLEDGMENTS

This work was supported by funding from the NASA Aeronautics Research Institute Seedling program.

■ REFERENCES

(1) Goodenough, J. B.; Kim, Y. Challenges for Rechargeable Li Batteries. *Chem. Mater.* **2010**, *22*, 587−603.

(2) Wang, H.; Liu, S.; Huang, K.; Yin, X.; Liu, Y.; Peng, S. $BMIMBF_4$ Ionic Liquid Mixtures Electrolyte for Li-ion Batteries. *Int. J. Electrochem. Sci.* **2012**, *7*, 1688−1698.

(3) Markevich, E.; Sharabi, R.; Borgel, V.; Gottlieb, H.; Salitra, G.; Aurbach, D.; Semrau, G.; Schmidt, M. A. *In Situ* FTIR Study of the Decomposition of N-butyl-N-methylpyrrolidinium Bis-(trifluoromethanesulfonyl)amide Ionic Liquid During Cathodic Polarization of Lithium and Graphite Electrodes. *Electrochim. Acta* **2010**, *55*, 2687−2696.

(4) Bhattacharyya, R.; Key, B.; Chen, H.; Best, A. S.; Hollenkamp, A. F.; Grey, C. P. *In Situ* NMR Observation of the Formation of Metallic Lithium Microstructures in Lithium Batteries. *Nat. Mater.* **2010**, *9*, 504−510.

(5) Schweikert, N.; Hofmann, A.; Schulz, M.; Scheuermann, M.; Boles, S. T.; Hanemann, T.; Hahn, H.; Indris, S. Suppressed Lithium Dendrite Growth in Lithium Batteries Using Ionic Liquid Electrolytes: Investigation by Electrochemical Impedance Spectroscopy, Scanning Electron Microscopy, and *In Situ* ^{7}Li Nuclear Magnetic Resonance Spectroscopy. *J. Power Sources* **2013**, *228*, 237−243.

(6) Best, A. S.; Bhatt, A. I.; Hollenkamp, A. F. Ionic Liquids with the Bis(fluorosulfonyl)imide Anion: Electrochemical Properties and Applications in Battery Technology. *J. Electrochem. Soc.* **2010**, *157*, A903−A911.

(7) Luntz, A. C.; McCloskey, B. D. Nonaqueous Li-Air Batteries: A Status Report. *Chem. Rev.* **2014**, *114*, 11721−11750.

(8) Manthiram, A.; Fu, Y.; Chung, S.-H.; Zu, C.; Su, Y.-S. Rechargeable Lithium-Sulfur Batteries. *Chem. Rev.* **2014**, *114*, 11751−11787.

(9) Lassègues, J. C.; Grondin, J.; Aupetit, C.; Johansson, P. Spectroscopic Identification of the Lithium Ion Transporting Species in LiTFSI-Doped Ionic Liquids. *J. Phys. Chem. A* **2009**, *113*, 305−314.

(10) Umebayashi, Y.; Mitsugi, T.; Fukuda, S.; Fujimori, T.; Fujii, K.; Kanzaki, R.; Takeuchi, M.; Ishiguro, S.-I. Lithium Ion Solvation in Room-Temperature Ionic Liquid Involving Bis-(trifluoromethanesulfonyl) Imide Anion Studied by Raman Spectroscopy and DFT Calculations. *J. Phys. Chem. B* **2007**, *111*, 13028−13032.

(11) Umebayashi, Y.; Hamano, H.; Seki, S.; Minofar, B.; Fujii, K.; Hayamizu, S.; ad Tsuzuki, K.; Kameda, Y.; Kohara, S.; Watanabe, M. Liquid Structure of and Li^+ Ion Solvation in Bis-(trifluoromethanesulfonyl)amide Based Ionic Liquids Composed of 1-Ethyl-3-methylimidazolium and N-Methyl-N-propylpyrrolidinium Cations. *J. Phys. Chem. B* **2011**, *115*, 12179−12191.

(12) Fujii, K.; Hamano, H.; Doi, H.; Song, X.; Tsuzuki, S.; Hayamizu, K.; Seki, S.; Kameda, Y.; Dokko, K.; Watanabe, M.; et al. Unusual Li^+ Solvation Structure in Bis(fluorosulfonyl)amide Based Ionic Liquid. *J. Phys. Chem. C* **2013**, *117*, 19314−19324.

(13) Pitawala, J.; Martinelli, A.; Johansson, P.; Jacobsson, P.; Matic, A. Coordination and Interactions in a Li-salt Doped Ionic Liquid. *J. Non-Cryst. Solids* **2015**, *407*, 318−323.

(14) Borodin, O. Polarizable Force Field Development and Molecular Dynamics Simulations of Ionic Liquids. *J. Phys. Chem. B* **2009**, *113*, 11463−11478.

(15) Castiglione, F.; Ragg, E.; Mele, A.; Appetecchi, G. B.; Montanino, M.; Passerini, S. Molecular Environment and Enhanced Diffusivity of Li^+ Ions in Lithium-Salt-Doped Ionic Liquid Electrolytes. *J. Phys. Chem. Lett.* **2011**, *2*, 153−157.

(16) Hayamizu, K.; Aihara, Y.; Nakagawa, H.; Nukuda, T.; Price, W. S. Ionic Conduction and Ion Diffusion in Binary Room-Temperature Ionic Liquids Composed of [emim][BF_4] and $LiBF_4$. *J. Phys. Chem. B* **2004**, *108*, 19527−19532.

(17) Solano, C. J. F.; Jeremias, S.; Paillard, E.; Beljonne, D.; Lazzaroni, R. A Joint Theoretical/Experimental Study of the Structure, Dynamics, and Li^+ Transport in Bis([tri]fluoro[methane]sulfonyl)-imide [T]FSI-based Ionic Liquids. *J. Chem. Phys.* **2013**, *139*, 034502.

(18) Zhang, Y.; Maginn, E. J. Direct Correlation between Ionic Liquid Transport Properties and Ion Pair Lifetimes: A Molecular Dynamics Study. *J. Phys. Chem. Lett.* **2015**, *6*, 700−705.

(19) Bortolini, O.; Chiappe, C.; Ghilardi, T.; Massi, A.; Pomelli, C. S. Dissolution of Metla Salts in Bis(trifluoromethylsulfonyl)imide-Based Ionic Liquids: Studying the Affinity of Metal Cations Toward a "Weakly Coordinating" Anion. *J. Phys. Chem. A* **2015**, *119*, 5078.

(20) Barnes, T. A.; Kaminski, J. W.; Borodin, O.; Miller, T. F., III *Ab Initio* Characterization of the Electrochemical Stability and Solvation Properties of Condensed-Phase Ethylene Carbonate and Dimethyl Carbonate Mixtures. *J. Phys. Chem. C* **2015**, *119*, 3865−3880.

(21) Ong, S. P.; Andreussi, O.; Wu, Y.; Marzari, N.; Ceder, G. Electrochemical Windows of Room-Temperature Ionic Liquids from Molecular Dynamics and Density Functional Theory Calculations. *Chem. Mater.* **2011**, *23*, 2979−2986.

(22) Ong, S. P.; Ceder, G. Investigation of the Effect of Functional Group Substitutions on the Gas-Phase Electron Affinities and Ionizations Energies of Room-Temperature Ionic Liquids Ions using Density Functional Theory. *Electrochim. Acta* **2010**, *55*, 3804−3811.

(23) Buijs, W.; Witkamp, G.-J.; Kroon, M. C. Correlation between Quantumchemically Calculated LUMO Energies and the Electrochemical Window of Ionic Liquids with Reduction-Resistant Anions. *Int. J. Electrochem.* **2012**, *2012*, 589050.

(24) Tian, Y.-H.; Goff, G. S.; Runde, W. H.; Batista, E. R. Exploring Electrochemical Windows of Room-Temperature Ionic Liquids: A Computational Study. *J. Phys. Chem. B* **2012**, *116*, 11943−11952.

(25) Zhang, Y.; Shi, C.; Brennecke, J. F.; Maginn, E. J. Refined Method for Predicting Electrochemical Windows of Ionic Liquids and Experimental Validation Studies. *J. Phys. Chem. B* **2014**, *118*, 6250−6255.

(26) Haskins, J. B.; Bennett, W. R.; Wu, J. J.; Hernández, D. M.; Borodin, O.; Monk, J. D.; Bauschlicher, C. W., Jr.; Lawson, J. W. Computational and Experimental Investigation of Li-Doped Ionic Liquid Electrolytes: [pyr14][TFSI], [pyr13][FSI], [EMIM][BF_4]. *J. Phys. Chem. B* **2014**, *118*, 11295−11309.

(27) Castiglione, F.; Famulari, A.; Raos, G.; Meille, S. V.; Appetecchi, G. B.; Passerini, S. Pyrrolidinium-Based Ionic Liquids Doped with Lithium Salts: How Does Li^+ Coordination Affect Its Diffusivity? *J. Phys. Chem. B* **2014**, *118*, 13679−13688.

(28) Nicotera, I.; Oliviero, C.; Henderson, W. A.; Appetecchi, G. B.; Passerini, S. NMR Investigation of Ionic Liquid-LiX Mixtures: Pyrrolidinium Cations and $TFSI^-$Anions. *J. Phys. Chem. B* **2005**, *109*, 22814−22819.

(29) Liu, H.; Maginn, E.; Visser, A. E.; Bridges, N. J.; Fox, E. B. Thermal and Transport Properties of Six Ionic Liquids: An Experimental and Molecular Dynamics Study. *Ind. Eng. Chem. Res.* **2012**, *51*, 7242−7254.

(30) Borodin, O.; Smith, G. D. Structure and Dynamics of N-methyl-N-propylpyrrolidinium Bis(trifluoromethanesulfonyl)imide Ionic Liquid from Molecular Dynamics Simulations. *J. Phys. Chem. B* **2006**, *110*, 11481−11490.

(31) Borodin, O.; Smith, G. D.; Henderson, W. Li^+ Cation Environment, Transport, and Mechanical Properties of the LiTFSI Doped N-Methyl-N-alkylpyrrolidinium$^+$ $TFSI^-$Ionic Liquids. *J. Phys. Chem. B* **2006**, *110*, 16879−16886.

(32) Liu, H.; Maginn, E. J. Effect of Ion Structure on Conductivity in Lithium-doped Ionic Liquid Electrolytes: a Molecular Dynamics Study. *J. Chem. Phys.* **2013**, *139*, 114508.

(33) Li, Z.; Smith, G. D.; Bedrov, D. Li^+ Solvation and Transport Properties in Ionic Liquid/Lithium Salt Mixtures: A Molecular Dynamics Simulation Study. *J. Phys. Chem. B* **2012**, *116*, 12801−12809.

(34) Ganesh, P.; Jiang, D.; Kent, P. R. C. Accurate Static and Dynamic Properties of Liquid Electrolytes for Li-Ion Batteries from Ab Initio Molecular Dynamics. *J. Phys. Chem. B* **2011**, *115*, 3085−3090.

(35) Ong, M. T.; Verners, O.; Draeger, E. W.; van Duin, A. C. T.; Lordi, V.; Pask, J. E. Lithium Ion Solvation and Diffusion in Bulk Organic Electrolytes from First-Principles and Classical Reactive Molecular Dynamics. *J. Phys. Chem. B* **2015**, *119*, 1535−1545.

DOI: 10.1021/acs.jpcb.5b06951
J. Phys. Chem. B 2015, 119, 14705−14719

(36) MacFarlane, D. R.; Meakin, P.; Sun, J.; Amini, N.; Forsyth, M. yrrolidinium Imides: A New Family of Molten Salts and Conductive Plastic Crystal Phases. *J. Phys. Chem. B* **1999**, *103*, 4164−4170.
(37) MacFarlane, D. R.; Sun, J.; Golding, J.; Meakin, P.; Forsyth, M. High Conductivity Molten Salts Based on the Imide Ion. *Electrochim. Acta* **2000**, *45*, 1271−1278.
(38) Appetecchi, G. B.; Montanino, M.; Balducci, A.; Lux, S. F.; Winterb, M.; Psserini, S. Lithium Insertion in Graphite from Ternary Ionic Liquid-Lithium Salt Electrolytes: 1. Electrochemical Characterization of the Electrolytes. *J. Power Sources* **2009**, *192*, 599−605.
(39) Khetan, A.; Pitsch, H.; Viswanathan, V. Identifying Descriptors for the Solvent Stability in Nonaqueous Li-O_2 Batteries. *J. Phys. Chem. Lett.* **2014**, *5*, 1318−1323.
(40) Borodin, O.; Olguin, M.; Spear, C. E.; Leiter, K. W.; Knap, J. Toward High Throughput Screening of Electrochemical Stability of Battery Electrolytes. *Nanotechnology* **2015**, *26*, 354003.
(41) Bauschlicher, C. W., Jr.; Haskins, J. B.; Bucholz, E. W.; Lawson, J. W.; Borodin, O. Structure and Energetics of Li^+-$(BF_4^-)_n$, Li^+-$(FSI_4^-)_n$, and Li^+-$(TFSI_4^-)_n$: *Ab Initio* and Polarizable Force Field Approaches. *J. Phys. Chem. B* **2014**, *118*, 10785−10794.
(42) Becke, A. D. Density-functional Thermochemistry III. The Role of Exact Exchange. *J. Chem. Phys.* **1993**, *98*, 5648−5652.
(43) Stephens, P. J.; Devlin, F. J.; Chabalowski, C. F.; Frisch, M. J. *Ab initio* Calculation of Vibrational Absorption and Circular Dichromism Spectra Using Density Functional Force Fields. *J. Phys. Chem.* **1994**, *98*, 11623−11627.
(44) Frisch, M. J.; Pople, J. A.; Binkley, J. S. Self-Consistent Molecular Orbital Methods. 25. Supplementary Functions for Gaussian Basis Sets. *J. Chem. Phys.* **1984**, *80*, 3265−3269.
(45) Frisch, M. J.; et al. *Gaussian 09*, Revision C.01; Gaussian, Inc.: Pittsburg, PA, 2009.
(46) Becke, A. D. Density-Functional Exchange-Energy Approximation with Correct Asymptotic-Behavior. *Phys. Rev. A: At., Mol., Opt. Phys.* **1988**, *38*, 3098−3100.
(47) Perdew, J. P.; Burke, K.; Ernzerhof, M. Generalized Gradient Approximation Made Simple. *Phys. Rev. Lett.* **1996**, *77*, 3865.
(48) Perdew, J. P.; Burke, K.; Ernzerhof, M. Erratum: Generalized Gradient Approximation Made Simple. *Phys. Rev. Lett.* **1997**, *78*, 1396.
(49) Heyd, J.; Scuseria, G. E.; Ernzerhof, M. Hybrid Functionals Based on a Screened Coulomb Potential. *J. Chem. Phys.* **2003**, *118*, 8207.
(50) Krukau, A. V.; Vydrov, O. A.; Izmaylov, A. F.; Scuseria, G. E. Influence of the Exchange Screening Parameter on the Performance of Screened Hybrid Functionals. *J. Chem. Phys.* **2006**, *125*, 224106.
(51) Zhao, Y.; Truhlar, D. G. The M06 Suite of Density Functionals for Main Group Thermochemistry, Thermochemical Kinetics, Noncovalent Interactions, Excited States, and Transition Elements: Two New Functionals and Systematic Testing of Four M06-Class Functionals and 12 Other Functionals. *Theor. Chem. Acc.* **2008**, *120*, 215−241.
(52) Kresse, G.; Hafner, J. *Ab Initio* Molecular Dynamics for Liquid Metals. *Phys. Rev. B: Condens. Matter Mater. Phys.* **1993**, *47*, 558.
(53) Kresse, G.; Hafner, J. *Ab Initio* Molecular-Dynamics Simulation of the Liquid-Metal-Amorphous-Semiconductor Transition in Germanium. *Phys. Rev. B: Condens. Matter Mater. Phys.* **1994**, *49*, 14251.
(54) Kresse, G.; Furthmüller, J. Efficiency of Ab Initio Total Energy Calculations for Metals and Semiconductors Using a Plane-Wave Basis Set. *Comput. Mater. Sci.* **1996**, *6*, 15.
(55) Kresse, G.; Furthmüller, J. Efficient IterativeSchemes for *Ab Initio* Total Energy Calculations Using a Plane-Wave Basis Set. *Phys. Rev. B: Condens. Matter Mater. Phys.* **1996**, *54*, 11169.
(56) Blochl, P. E. Projector Augmented-Wave Method. *Phys. Rev. B: Condens. Matter Mater. Phys.* **1994**, *50*, 17953.
(57) Kresse, G.; Joubert, D. From Ultrasoft Pseudopotentials to the Projector Augmented-Wave Method. *Phys. Rev. B: Condens. Matter Mater. Phys.* **1999**, *59*, 1758.
(58) Borodin, O.; Smith, G. D. Development of Many-Body Polarizable Force Fields for Li-Battery Components: 1. Ether, Alkane, and Carbonate-Based Solvents. *J. Phys. Chem. B* **2006**, *110*, 6279−6292.
(59) Borodin, O.; Smith, G. D. Development of Many-Body Polarizable Force Fields for Li-Battery Applications: 2. LiTFSI-Doped Oligoether, Polyether, and Carbonate-Based Electrolytes. *J. Phys. Chem. B* **2006**, *110*, 6293−6299.
(60) Plimpton, S. *J. Comput. Phys.* **1995**, *117*, 1−19. see http://lammps.sandia.gov.
(61) Borodin, O.; Smith, G. D. Development of Many-Body Polarizable Force Fields for Li-Battery Applications: 2. LiTFSI-Doped Oligoether, Polyether, and Carbonate-Based Electrolytes. *J. Phys. Chem. B* **2006**, *110*, 6293−6299.
(62) Johansson, P.; Gejji, S. P.; Tegenfeldt, J.; Lindgren, J. The Imide Ion: Potential Energy Surface and Geometries. *Electrochim. Acta* **1998**, *43*, 1375−1379.
(63) Gejji, S. P.; Suresh, C. H.; Babu, K.; Gadre, S. R. *Ab Initio* Structure and Vibrational Frequencies of $(CF_3SO_2)_2N^-Li^+$ Ion Pairs. *J. Phys. Chem. A* **1999**, *103*, 7474−7480.
(64) Fujii, K.; Fujimori, T.; Takamuku, T.; Kanzaki, R.; Umebayashi, Y.; Ishiguro, S.-I Conformational Equilibrium of Bis(trifluoromethanesulfonyl) Imide Anion of a Room-Temerature Ionic Liquid: Raman Spectroscopic Study and DFT Calculations. *J. Phys. Chem. B* **2006**, *110*, 8179−8183.
(65) Herstedt, M.; Smirnov, M.; Johansson, P.; Chami, M.; Grondin, J.; Servant, L.; Lassègues, J. C. Spectroscopic Characterization of the Conformational States of the Bis(trifluromethanesulfonyl)imide Anion $(TFSI)^-$. *J. Raman Spectrosc.* **2005**, *36*, 762−770.
(66) Andreussi, O.; Marzari, N. Transport Properties of Room-Temperature Ionic Liquids from Classical Molecular Dynamics. *J. Chem. Phys.* **2012**, *137*, 044508.
(67) Lewandowski, A.; Stepniak, I. Relative Molar Gibbs Energies of Cation Transfer from a Molecular Liquid to Ionic Liquids at 298.15 K. *Phys. Chem. Chem. Phys.* **2003**, *5*, 4215−4218.
(68) Noda, A.; Watanabe, M. Highly Conductive Polymer Electrolytes Prepared by *In Situ* Polymerization of Vinyl Monomers in Room Temperature Molten Salts. *Electrochim. Acta* **2000**, *45*, 1265−1270.
(69) Fuller, J.; Carlin, R. T.; Osteryoung, R. A. The Room Temperature Ionic Liquid 1-Ethyl-3-Methylimidazolium Tetrafluoroborate: Electrochemical Couples and Physical Properties. *J. Electrochem. Soc.* **1997**, *144*, 3881−3886.

DOI: 10.1021/acs.jpcb.5b06951
J. Phys. Chem. B 2015, 119, 14705−14719